A Common Formalism for Isotropic vs. Anisotropic Models for Porosity Effects on X-ray Line Profiles

Stan Owocki

Bartol Research Institute, University of Delaware, Newark, DE 19716

DRAFT NOTES, version of February 27, 2006

1. Background

In her email of Feb. 7, Lida (Oskinova) comments on our recent OC06 preprint on the effect of porosity for X-ray line profiles, particularly in relationship to the Oskinova, Feldmier, & Hamman (OFH) model for a "fractured wind" made up of radially compressed "pancakes". It seems in particular that the OC06 "porosity" length has a potentially close correspondence to the radial separation distance between the thin pancakes in the OFH model. There moreover seems to be a potential emerging consensus that reducing b-f absporption to a level that can give the observed, nearly symmetric X-ray profiles requires quite large separations or porosity lengths, i.e. $h > R_*$.

Spurred by this prospect of a congenial reconcilation of what has been till now two rather different perpsectives, I have recently implemented this pancake formalism within my general Mathematica analysis of porosity, with the aim to compare line profiles for the two models of porosity.

2. OFH Radially Compressed Pancake Model for Anisotropic Porosity

In the OFH model, the individual pancakes are assumed to be geometrically thin, with a local radial separation h between pancakes. For a wind with local average density ρ, the pancake column density is ρh. Thus with radially oriented pancakes, the optical depth of the pancake to a ray with radial direction cosine μ is

$$\tau_c = \kappa \rho h / \mu \,. \tag{1}$$

In the OFH model, the pancakes are assumed to be released at a fixed temporal frequency n_o, and so they then spread spatially according to the accelerating velocity of the wind, given by a beta-law. The radial variation of the shell separation can thus be written in the form

$$h(r) = v(r)/n_o = h_\infty (1 - R/r)^\beta \,, \tag{2}$$

where $h_\infty \equiv v_\infty/n_o$ is the asymptotic radial separation between clumps at large radii, given in terms of the clump release frequency n_o and the terminal flow speed v_∞. Also, R is the stellar radius, and, for simplicity, our analysis here will take a velocity exponent $\beta = 1$.

For this anisotropic porosity, we will find it more convenient to use the absorption form for the effective opacity, as given by, e.g., eqn. (4) of OC06,

$$\frac{\kappa_{eff}}{\kappa} = \frac{1 - e^{-\tau_c}}{\tau_c} \,. \tag{3}$$

The effective optical depth integral (analagous to eqn. (7) of OC06), to a position z along a ray with impact parameter p is now written as,

$$t_{eff}[p,z] = \int_z^\infty \left(1 - e^{-\tau_c(z')}\right) \frac{\kappa\rho}{\kappa\rho h/\mu}\, dz' \tag{4}$$

$$= \int_r^\infty \left(1 - e^{-\tau_c(r')}\right) dr'/h(r') \tag{5}$$

where the latter simplification uses the relations $z^2 \equiv r^2 - p^2$ and $\mu = z/r$ to substitute $dz' = dr'r'/z' = dr'/\mu$. This shows that the optical depth of the region where the clumps are optically thick is just given by the *number* of radial clumps separations crossed along the path.

For evaluating this integral, it is reasonable to approximate the 1-e factor as a step function, with the step occuring at the radius r_1 where the clumps along a given ray with impact parameter p become optically thick, defined by $\tau_c(r_1) \equiv 1$. In terms of the ray coordinate $z_1 = \sqrt{r_1^2 - p^2}$, this requirement can be written as

$$z_1 r_1 = \tau_* h_\infty \,, \tag{6}$$

where

$$\tau_* \equiv \frac{\kappa \dot{M}}{4\pi v_\infty R} \,, \tag{7}$$

and for convenience, we are scaling all lengths in units of the stellar radius R. The requirement can be solved explicitly to give

$$z_1(p, \tau_* h_\infty) = \sqrt{-p^2 + \sqrt{p^4 + 4\tau_*^2 h_\infty^2}} \,. \tag{8}$$

The corresponding radius can obtained from $r_1 = \sqrt{p^2 + z_1^2}$. Figure 1 plots z_1 vs. p for various $\tau_* h_\infty$.

For the intervals $r > r_1(p)$, the ray optical depth integral recovers the form for a *smooth* wind, which for a simple ('beta=1') velocity law, can be evaluated though analytic form (see,

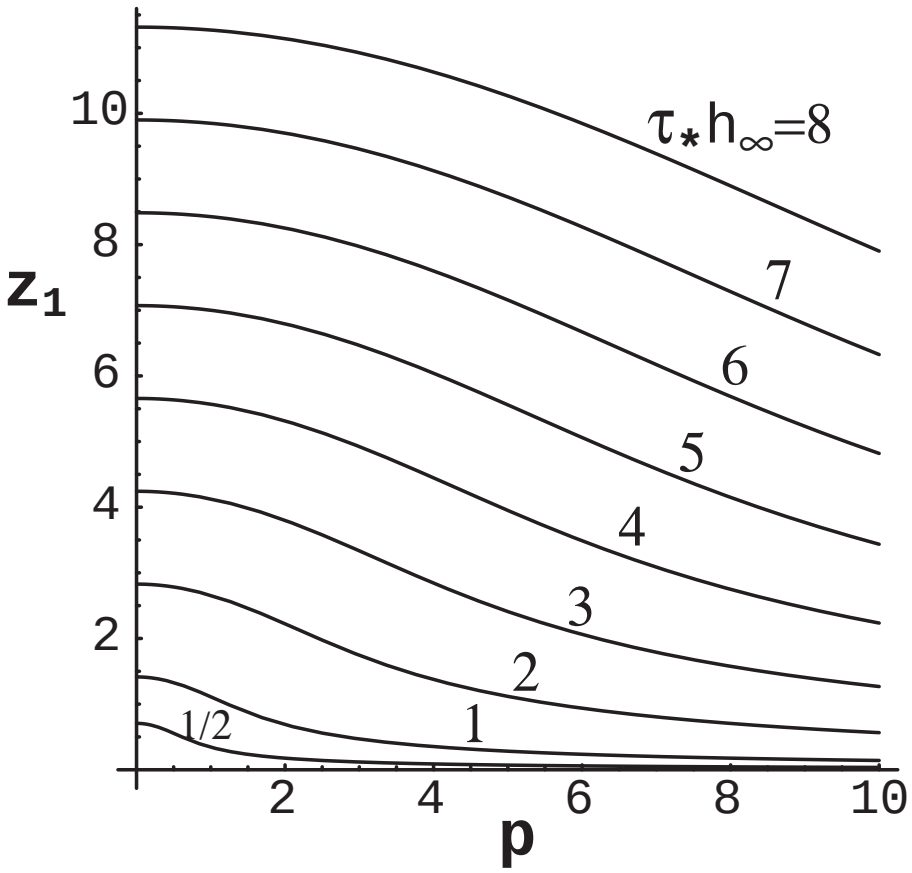

Fig. 1.— Plot of $z_1(p, \tau_* h_\infty)$ vs. impact parameter p for various $\tau_* h_\infty$ (0.5 and from 1 to 8, in unit steps), showing location where pancakes become marginally optically thick to photons along the ray with associated impact parameter p.

e.g., OC01 and OC06),

$$t_{sm}[p,z,z'] = \frac{1}{z_*}\left[\arctan\left(\frac{z'}{z_*}\right) + \arctan\left(\frac{z'}{r'z_*}\right)\right]_z^{z'} , \tag{9}$$

where $z_* \equiv \sqrt{p^2-1}$.

For the intervals $r < r_1$, the integral just represents a summation over the shell separation lengths h; in the present case of $h(r) \sim v(r)$ with $\beta = 1$, the integration gives the analytic form

$$t_{an}[p,z,z'] = \frac{1}{h_\infty}\left[r + \log(r-1)\right]_z^{z'} . \tag{10}$$

The overall effective optical depth can thus be written

$$\begin{aligned}
\frac{t_{eff}[p,z]}{\tau_*} &= t_{sm}[p,z,\infty] \quad ; \quad z \geq z_1 && (11)\\
&= t_{an}[p,z,z_1] + t_{sm}[p,z_1,\infty] \;\; ; \;\; 0 \leq z \leq z_1 && (12)\\
&= t_{an}[p,z,0] + t_h[p,0,z_1] + t_{sm}[p,z_1,\infty] \;\; ; \;\; -z_1 \leq z \leq 0 && (13)\\
&= t_{an}[p,z,-z_1] + t_h[p,-z_1,0] + t_{an}[p,0,z_1] + t_{sm}[p,z_1,\infty] \;\; ; \;\; z \leq -z_1 && (14)
\end{aligned}$$

With the ray optical depths in hand, we can readily convert to optical depth as a function of radius and direction. Using the scaled velocity law $w \equiv v/v_\infty = (1 - R/r)$, this can then be converted to a function of scaled inverse radius $y = 1 - 1/r$, and scaled wavelength $x = (\lambda/\lambda_o - 1)c/v_\infty$.

3. Optical Depth for a "Stretch" Form for Isotropic Porosity

Before computing X-ray line profiles, let us consider a hybrid form for the previous OC06 isotropic porosity model. Specifically, instead the OC06 assumption that the porosity length *expands* in proportion to the local radius, $h(r) = h'r$, let us assume that, in ananlogy with the above formulation OFH anisotropic model, the porosity length *stretches* with the wind flow speed, $h(r) = h_\infty v(r)/v_\infty = h_\infty(1 - 1/r)$ (where we have again taken a simple $\beta = 1$ form for the velocity law).

We will thus dub these respectively the "expansion" vs. "stretch" forms for isotropic porosity.

For the OF06 form for the porosity "bridging law", the ray optical depth for an isotropic stretch porosity model becomes (cf. OC06 eqn. (9))

$$\frac{t_{eff}[p,z]}{\tau_*} = \int_z^\infty \frac{dz'}{(r'^2 + \tau_* h_\infty)(1 - 1/r')} , \tag{15}$$

where we are still writing all lengths in units of the stellar radius R. Fortunately, in this case the integral can also be evaluated analytically, yielding

$$\frac{t_{eff}[p,z]}{\tau_*} = \frac{t_{sm}[p,z,\infty] + \tau_* h_\infty \, t_{iso}[p,z,\infty]}{1+\tau_* h_\infty} \tag{16}$$

where t_{sm} is defined in eqn. (9) above, and

$$t_{iso}[p,z,\infty] \equiv \frac{1}{z_h}\left[\arctan\left(\frac{z'}{z_h}\right) + \frac{\arctan\left(\frac{\sqrt{\tau_* h_*}z'}{z_h r'}\right)}{\sqrt{\tau_* h_*}}\right]_{z'=z}^{z'\to\infty}, \tag{17}$$

with $z_h \equiv \sqrt{p^2+\tau_* h_\infty}$.

4. X-ray Line Profiles for Anisotropic vs. Isotropic Porosity Models

With these analytic optical depth expressions in hand, we can model the associated X-ray emission line profiles using the parameterized emission model introduced by OC01. As in OC06, we focus here on the simple case of pure density-squared emission ($q = 0$) beginning at a minimum emission radius $R_{min} = 1.5R$.

Figure 2 compares results for the anisotropic porosity model (right column) with the expansion and stretched forms of the isotropic porosity (left and middle columns). As in OC06 (cf. their figure 3), the curves show X-ray line profiles vs. scaled wavelength $x \equiv (\lambda/\lambda_o - 1)c/v_\infty$, overplotted in each panel for optical depth parameters $\tau_* = 0.1$, 1, 3, 5, and 10 (black, blue, violet, red, green), and normalized to have peaks decrease by 5% for each step in τ_*. The individual panels compare results for various porosity scales and models. For all three model columns, the rows show results for increasing porosity scale, i.e. h' or h_∞, with values as labeled at the left of each row. The vertical dashed lines mark the line centers.

Note that the profiles for all 3 porosity models are generally quite similar for comparable porosity scales, although there are some some differences in details. For example, in the anistropic models, the increase in intensity occurs first near line center, reflecting the greater transverse transmission of radiation through the midplane between the front and back hemispheres. Because the expansion form of the isotropic model has a porosity that continues to increase with radius, for a given scale factor, the overall symmetrization of the profile is greatest in this model. However, in comparing the two models with the velocity stretch scaling of porosity, the symmetrization is stronger for the anisotropic case, indicating that assuming such a "pancake" form for the clumps does indeed somewhat enhance porosity effects.

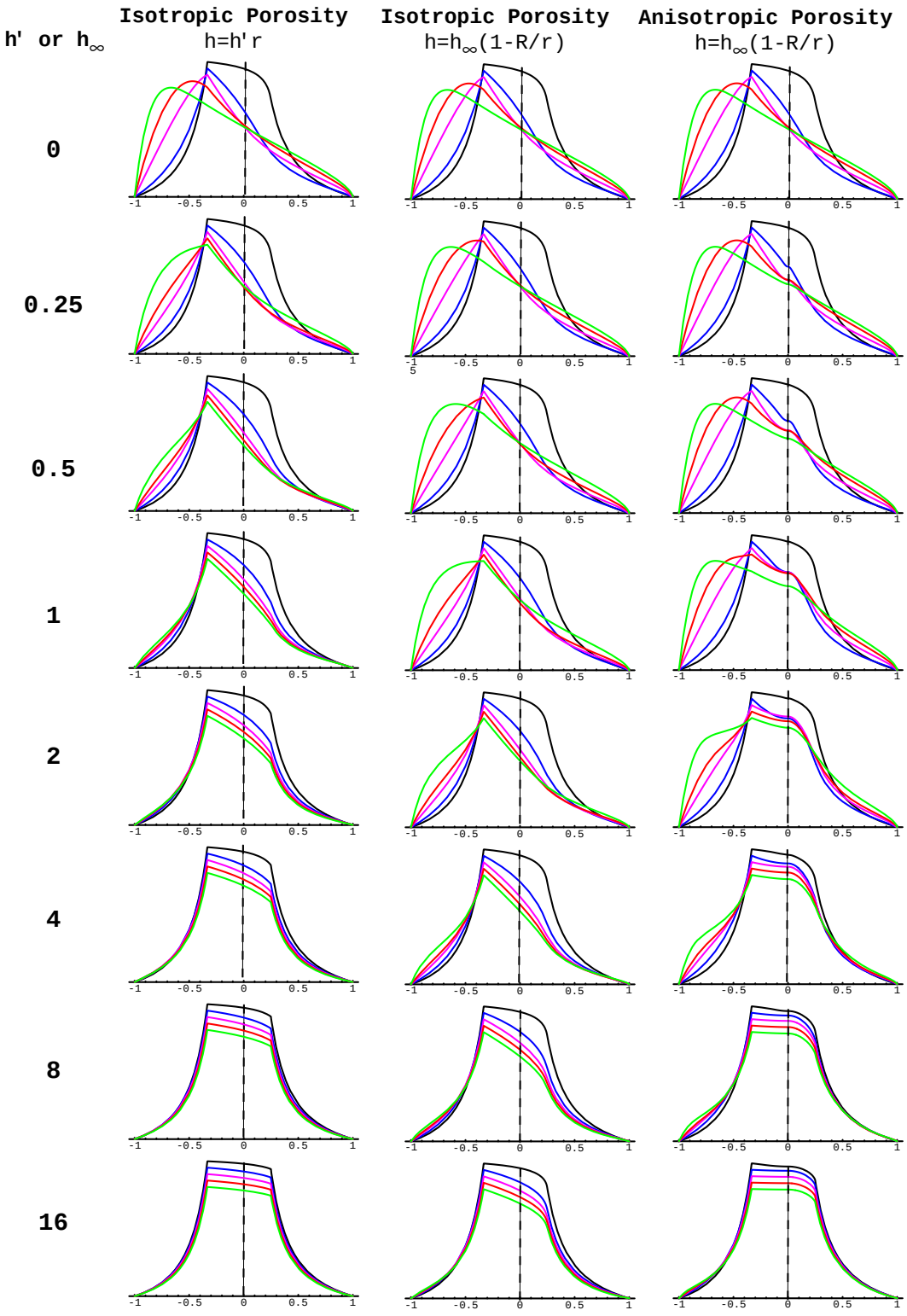

Fig. 2.— Comparison of X-ray line profiles for this anistropic porosity model (right column) vs. analogous expansion (left) and stretch (middle) forms for isotropic porosity models See text for details.

Nonetheless, in all models, achieving nearly symmetric profiles for optically thick cases ($\tau_* \geq 1$) requires quite large porosity lengths, $h > R_*$ or more.

Overall, these results thus seem to point to a reconciliation between the OFH anisotropic pancake model and the OC06 isotoropic porosity model, with the OFH radial separation length between clumps playing a similar role to the OC06 "porosity length". The correspondence is particularly close if one uses the velocity stretch form for the spatial variation of the OC06 porosity length, $h(r) = h_\infty v(r)/v_\infty$, instead of radial expansion form $h(r) = h'r$.

Finally, I have also developed Mathematica code for computing X-ray line profiles from models consisting of spherically symmetric thin shells. It turns out that, even with relatively large shell separations, such models do not generally give very symmetric line profiles. This shows that the lateral reshuffling associated with the pancake model is quite essential to obtaining the reduced absorption of a porosity model. I may add further details of these shell model profiles to later versions of these notes.